IV. ELECTRODYNAMICS OF MEDIA

Academic and Research Staff

Prof. W. P. Allis
Prof. H. J. Carlin
Prof. L. J. Chu
Prof. H. A. Haus
Prof. J. A. Kong
Prof. P. Penfield, Jr.
Prof. D. H. Staelin
Dr. A. H. M. Ross

Graduate Students

C. P. Ausschnitt
E. L. Frohring
T. Holcomb
E. W. Maby
J. L. Miller
W. A. Stiehl
L. Tsang
P. S. K. Wong

A. ELECTRON DISTRIBUTION AND PUMPING IN A CO_2 LASER MODEL

Joint Services Electronics Program (Contract DAAB07-71-C-0300)

U. S. Army Research Office – Durham (Contract DAHC04-72-C-0044)

H. A. Haus, W. P. Allis

In a previous report,[1] we developed a theory for the electron distribution in a diatomic gas laser and its interaction with the population distribution of the lasing species. Such an analysis is necessary to obtain analytic expressions for the power output and efficiency of a laser. In the present report we extend the analysis to describe a model for the CO_2 laser.

For mathematical simplicity, we adopt a model in which the molecular gas is represented by two temperatures. For this purpose, we consider the nitrogen vibrational levels to be tightly coupled to the asymmetric stretching mode of CO_2 and treat the two vibrational systems as one. Similarly, we assume that the symmetric stretching mode of CO_2 is tightly coupled to the bending mode and that both of these can be described by a single vibrational temperature. Furthermore, we assume that the nitrogen vibrational mode and the asymmetric stretching mode of CO_2 are excited via an intermediate ionic state so that excitation occurs when the electrons have reached a critical energy u_a (~2 eV); in excitation they are assumed to lose a fraction, Δu, of this energy. We assume that the excitation of the combined system of symmetric stretching and bending modes is effected by low-energy electrons that lose an energy V_b upon excitation. Under these simplifying assumptions, closed-form expressions can be derived for all physical quantities of interest.

1. Electron Distribution

The distribution function of the electrons f(u) in energy space is obtained analogously to the derivation in our previous report.[1] We supplement the current in

energy space, the G-function, with the contribution of the combined bending symmetric stretching mode excitation characterized by an excitation frequency ν_b. The differential equation for the distribution function f(u), in which we have disregarded elastic losses, becomes ($u_b^- \equiv u_b - V_b$)

$$-\frac{2}{3}\frac{e}{m}\left(\frac{E}{\nu_m}\right)^2 \nu_m u^{3/2}\frac{df}{du} = \nu_x + \Delta u \nu_a \delta(u-u_a); \qquad u_b < u \leq u_x$$

$$= \nu_x + \Delta u \nu_a \delta(u-u_a) + \nu_b; \qquad u_b^- < u \leq u_b. \tag{1}$$

Here E is the applied electric field, ν_m is the frequency of momentum-changing collisions, ν_x is the frequency of electronic excitations assumed to occur when the electrons reach energy u_x, ν_a is the excitation frequency of the intermediate ionic state

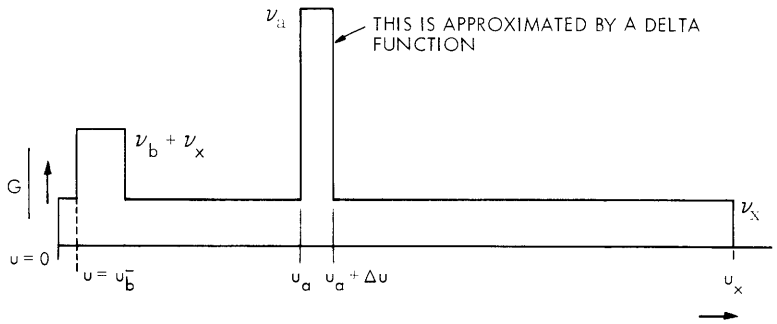

Fig. IV-1. Current in energy space (G-function).
$u_b \approx 0.05$ eV
$u_a \approx 2$ eV
$\Delta u \approx 0.2$ eV
$u_x \approx 10$ eV.

which then leads to an excitation of the combined asymmetric stretching mode and nitrogen vibrational levels, and ν_b is the frequency of excitation of the combined bending and symmetric stretching modes which occurs when the electrons reach energy u_b. We use subscript a for the process which is analogous to that denoted by subscript e in our previous report.[1] Figure IV-1 illustrates the G-function. We introduce a definition for drift energy u_d given by

$$u_d \equiv \frac{1}{2}\frac{e}{m}\left(\frac{E}{\nu_m}\right)^2. \tag{2}$$

Equation 1 permits a closed-form solution for the distribution function

$$f(u) = \frac{\nu_x}{\nu_m}\frac{3}{2u_d}\left\{\frac{1}{\sqrt{u}} - \frac{1}{\sqrt{u_x}}\right\}; \qquad u_a < u \leq u_x$$

$$f(u) = \frac{\nu_x}{\nu_m}\frac{3}{2u_d}\left\{\frac{1}{\sqrt{u}} - \frac{1}{\sqrt{u_x}} + \frac{\nu_a}{\nu_x}\frac{\Delta u}{2u_a^{3/2}}\right\}; \qquad u_b < u \leq u_a$$

$$f(u) = \frac{\nu_x}{\nu_m}\frac{3}{2u_d}\left\{\frac{1}{\sqrt{u}} - \frac{1}{\sqrt{u_x}} + \frac{\nu_a}{\nu_x}\frac{\Delta u}{2u_a^{3/2}}\right\} + \frac{\nu_b}{\nu_m}\frac{3}{2u_d}\left\{\frac{1}{\sqrt{u}} - \frac{1}{\sqrt{u_b}}\right\}; \qquad u_b < u \leq u_b. \tag{3}$$

If we introduce the normalization condition

$$\int \sqrt{u}\ f(u)\, du = 1, \tag{4}$$

we obtain a relationship among the different excitation frequencies

$$\nu_x u_x + \nu_a \Delta u + \nu_b V_b = \nu_m 2u_d. \tag{5}$$

Equation 5 is a form of the energy conservation law. On the left-hand side is the rate of energy loss by the electrons, per electron, and on the right-hand side is the rate of energy supply by the electric field to the electrons, per electron. Equation 5 is one equation for the three unknowns, ν_x, ν_a, ν_b for a given electric field E. In order to find more relationships the molecular excitation has to be studied in greater detail.

2. Molecular Excitation

We assume that the distribution of CO_2 over the asymmetric stretching mode (and the nitrogen vibrational distribution), the symmetric stretching mode, and the bending mode are all described in terms of vibrational temperatures. We introduce convenient energy parameters,

$$a \equiv \exp(-\hbar\omega_a/kT_a) \qquad b \equiv \exp(-\hbar\omega_b/kT_b) \qquad s \equiv \exp(-\hbar\omega_s/kT_b). \tag{6}$$

Note that the energy parameter for the symmetric stretching mode s is equal to the square of that of the bending mode, $s = b^2$, because the assumption is made that the spacing of the energy levels of the symmetric stretching mode is twice that of the bending mode, and that the temperatures of the two modes are the same. It is helpful to introduce additional energy parameters by definition:

$$\frac{\alpha}{1+\alpha} \equiv a \qquad \frac{\beta}{1+\beta} \equiv b \qquad \frac{\sigma}{1+\sigma} \equiv s. \tag{7}$$

The energy U in a particular mode, when it is nondegenerate, is given directly in terms of Greek letters; for example, $U_a = \hbar\omega_a \alpha$. The energy conservation relation for the asymmetric stretching mode can be written conveniently in the form

$$n_e \nu_a = NC_{MN}\left\{\frac{d\alpha}{dt} + \frac{\alpha - \alpha_g}{\tau_a} - R\right\}, \qquad \text{where} \quad \alpha_g = \frac{1}{\exp(\hbar\omega_a/kT_g) - 1}. \tag{8}$$

Here τ_a is a phenomenological relaxation time for the asymmetric stretching mode, R is the rate at which vibrational quanta are lost from the system via radiative transitions, n_e is the electron density, and N is the particle density. C_{MN} is the mole fraction of nitrogen and CO_2 because α describes the combined energy of the asymmetric stretching mode and the nitrogen vibrational mode. In order to write an energy conservation relation for the symmetric stretching mode and the bending mode it is necessary to take note of the degeneracy of the bending mode. The m^{th} level of the bending mode has degeneracy m+1. Under these conditions the energy in the bending mode is $2\beta\hbar\omega_b$. By using this fact, the energy conservation relation for the combined symmetric stretching and bending modes becomes

$$n_e \nu_b = NC_M\left\{\frac{d}{dt}(\sigma+2\beta) + \frac{\alpha - \alpha_g}{\tau_s} + \frac{2(\beta-\beta_g)}{\tau_b} + R\right\}. \tag{9}$$

Here we have introduced the two phenomenological relaxation times τ_s and τ_b for the stretching and bending modes, respectively. C_M is the mole fraction of CO_2. The arrival of quanta via radiative transitions is contained in R. Since σ is related to β by

$$\frac{\sigma}{1+\sigma} = \left(\frac{\beta}{1+\beta}\right)^2, \tag{10}$$

Eqs. 8 and 9 provide two relations for the two unknowns α and β in terms of ν_a and ν_b. Now the excitation frequencies themselves depend on the molecular excitation. One of these dependencies can be taken directly from our previous report.[2] In the present report we have changed the subscript e to a. Also, we have defined a new parameter ξ, proportional to the collision cross section that incorporates some of the parameters that we have defined. Finally,

$$u'_a \equiv 2u_a\left(1 - \sqrt{\frac{u_a}{u_x}}\right).$$

The excitation rate of the combined asymmetric stretching mode and the nitrogen vibrational mode is

$$\frac{\nu_a}{\nu_x} = \xi \frac{\frac{u_x}{2u_d}}{1 + \xi a \frac{\Delta u}{2u_d} \frac{u_x}{u'_a}}, \tag{11}$$

which is obtained from an assumed dipolar collision model for the molecules treated as harmonic oscillators.

Now, consider the excitation of the bending mode, and in particular, the de-excitation of the $(m+1)^{th}$ level to the m^{th} level by an electron collision, as a result of which the m^{th} level's population is increased.

Assuming that the electron collision cross section is $Q(v)$, we have for the rate of excitation of the fractional population x_m per degenerate mode, x_m/g_m (where g_m is the degeneracy), by entry of particles from the level m+1,

$$(m+1) \frac{x_{m+1}}{g_{m+1}} \int v^2 n_e v Q_{10}(v) f(v) dv. \tag{12}$$

The factor (m+1) arises because we assume interaction of the electron with the molecule via an induced dipole of the molecule. Perturbation analysis shows that the cross section for the $m+1 \rightarrow m$ transition is proportional to m+1. Furthermore, the rate is proportional to the fractional population per degenerate energy level of the $(m+1)^{th}$ level. The term $vQ_{10}(v)\, n_e$ is the collision frequency for a $1 \rightarrow 0$ transition. This expression can be conveniently written in terms of the distribution function f(u)

$$n_e(m+1) \frac{x_{m+1}}{g_{m+1}} \int \sqrt{u}\, f(u)\, R_{10}(u)\, du, \tag{13}$$

where $R_{10}(u)$ is $vQ_{10}(v)$ as a function of u.

In this format it is easy to take account of the Klein-Rossland relation which states that the rate of up-transitions from the m^{th} level to the $(m+1)^{th}$ level is related to the rate of down transitions, in that the f(u) of (13) has to be replaced by $f(u+u_b)$, where u_b is the energy loss in a collision. Taking these relations into account, we have

$$\left(\frac{d}{dt} \frac{x_m}{g_m}\right)_{\text{electrons}} = n_e \left\{(m+1) \frac{x_{m+1}}{g_{m+1}} \int_0^\infty \sqrt{u}\, f(u)\, R_{10}(u)\, du \right.$$

$$- \left[(m+1) \int_0^\infty \sqrt{u}\, f(u+V_b)\, R_{10}(u)\, du + m \int_0^\infty \sqrt{u}\, f(u)\, R_{10}(u)\, du\right] \frac{x_m}{g_m}$$

$$\left. + m \frac{x_{m-1}}{g_{m-1}} \int_0^\infty \sqrt{u}\, f(u+V_b)\, R_{10}(u)\, du \right\}. \tag{14}$$

If we assume that the V-V coupling is so strong that thermal equilibrium is established in the bending mode, we may set

$$x_m = (m+1)(1-b)^2\, b^m \tag{15}$$

and obtain the rate of energy transfer from the electrons to the vibrational mode by multiplying both sides of (14) by u_b and g_m and adding over all m. The result may be identified with the rate of energy supply per molecule, by multiplying with $\Delta u\, n_e \nu_b / NC_M$. After carrying out the summation, we have

$$\Delta u\, \frac{n_e \nu_b}{NC_M} = \Delta u\, n_e 2\left(\frac{1+b}{1-b}\right)\left[\int_0^\infty \sqrt{u}\; f(u+V_b)\; R_{10}(u)\, du - b\int_0^\infty \sqrt{u}\; f(u)\; R_{10}(u)\, du\right]. \tag{16}$$

As a simplifying assumption we take $R_{10}(u)$ as a unit impulse (delta) function at the energy $u = \bar{u_b}$

$$R_{10}(u) = R\delta\left(u-\bar{u_b}\right).$$

Now we may introduce the expressions for f(u) and obtain for the integrals

$$\int \sqrt{u}\; f(u+V_b)\; R_{10}(u)\, du = R\,\frac{3}{2u_d}\left[\frac{\nu_x}{\nu_m}\left(\left(\frac{\bar{u_b}}{u_b}\right)^{1/2} - \left(\frac{u_b}{u_x}\right)^{1/2}\right) + \frac{\nu_a}{\nu_m}\,\frac{\Delta u\sqrt{\bar{u_b}}}{2u_a^{3/2}}\right]$$

and

$$\int \sqrt{u}\; f(u)\; R_{10}(u)\, du = R\,\frac{3}{2u_d}\left[\frac{\nu_x}{\nu_m}\left(1 - \left(\frac{\bar{u_b}}{u_x}\right)^{1/2}\right) + \frac{\nu_a}{\nu_m}\,\frac{\Delta u\sqrt{\bar{u_b}}}{2u_a^{3/2}} + \frac{\nu_b}{\nu_m}\left(1 - \sqrt{\frac{\bar{u_b}}{u_b}}\right)\right].$$

Introducing these expressions into (16), we obtain

$$\frac{\nu_b}{\nu_m} = 2\,\frac{NC_M}{\nu_m}\,\frac{3}{2u_d}\,R\left(\frac{1+b}{1-b}\right)\left\{\frac{\nu_x}{\nu_m}\left[\left(\frac{\bar{u_b}}{u_b}\right)^{1/2} - b - (1-b)\left(\frac{\bar{u_b}}{u_x}\right)^{1/2}\right]\right.$$

$$\left. + \frac{\nu_a}{\nu_m}(1-b)\,\Delta u\,\frac{\sqrt{\bar{u_b}}}{2u_a^{3/2}} - b\,\frac{\nu_b}{\nu_m}\left(1 - \sqrt{\frac{\bar{u_b}}{u_b}}\right)\right\}. \tag{17}$$

We may define a dimensionless parameter η which is a measure of the collision cross section for excitation of the bending mode (the precise meaning of η will soon become apparent).

$$\eta = \frac{6NC_M}{u_x \nu_m} R. \tag{18}$$

In terms of this parameter, we have

$$\frac{\nu_b}{\nu_m} = \frac{\eta\left(\frac{1+b}{1-b}\right)\left\{\frac{\nu_x}{\nu_m}\left[\left(\frac{\bar{u_b}}{u_b}\right)^{1/2} - b - (1-b)\left(\frac{\bar{u_b}}{u_x}\right)^{1/2}\right] + \frac{\nu_a}{\nu_m}(1-b)\frac{\Delta u\sqrt{\bar{u_b}}}{2u_a^{3/2}}\right\}\frac{u_x}{2u_d}}{1 + \eta b\left(\frac{1+b}{1-b}\right)\frac{u_x}{2u_d}\left(1 - \sqrt{\frac{\bar{u_b}}{u_b}}\right)}. \tag{19}$$

The remaining equations for rates ν_x, ν_a, and ν_b are (5) and (11). Solving for ν_x/ν_m, we find

$$\frac{\nu_x}{\nu_m} = \frac{2u_d}{u_x}\left\{\left[1 + \xi\frac{\frac{\Delta u}{2u_d}}{1 + \xi a\frac{\Delta u}{2u_d}\frac{u_x}{u'_a}}\right]\left[1 + \eta b\left(\frac{1+b}{1-b}\right)\frac{u_x}{2u_d}\left(1 - \sqrt{\frac{\bar{u_b}}{u_b}}\right)\right]\right.$$

$$\left. + \frac{V_b}{2u_d}\eta\left(\frac{1+b}{1-b}\right)\left[\frac{\Delta u}{2u_a}\sqrt{\frac{\bar{u_b}}{u_a}}(1-b)\xi\frac{\frac{u_x}{2u_d}}{1 + \xi a\frac{\Delta u}{2u_d}\frac{u_x}{u'_a}} + \sqrt{\frac{\bar{u_b}}{u_b}} - b - (1-b)\sqrt{\frac{\bar{u_b}}{u_x}}\right]\right\}^{-1} \tag{20}$$

Equations (5) and (11) may then serve to find ν_b/ν_m and ν_a/ν_m.

It is of interest to study the behavior of the rates when the molecular system is in the ground state. Furthermore, consider the limits of low and high E-field $u_d \to 0$, and $u_d \to \infty$.

In the limit $u_d \to 0$,

$$\left.\frac{\nu_b}{\nu_m}\right|_{u_d \to 0} = \frac{2u_d}{V_b} \tag{21}$$

$$\left.\frac{\nu_a}{\nu_m}\right|_{u_d \to 0} = \frac{(2u_d/u_x)^2}{\eta\frac{V_b}{u_x}\frac{\Delta u\sqrt{\bar{u_b}}}{2u_a^{3/2}}} \tag{22}$$

$$\frac{\nu_x}{\nu_m}_{u_d \to 0} = \frac{(2u_d/u_x)^3}{\xi\eta \frac{V_b}{u_x} \frac{\Delta u \sqrt{u_b^-}}{2u_a^{3/2}}}. \tag{23}$$

In the limit $u_d \to \infty$,

$$\frac{\nu_b}{\nu_m} = \eta \left(\sqrt{\frac{u_b^-}{u_b}} - \sqrt{\frac{u_b^-}{u_x}} \right) \approx \eta \sqrt{\frac{u_b^-}{u_b}} \tag{24}$$

because $u_b^- \ll u_x$.

$$\frac{\nu_a}{\nu_m} = \xi. \tag{25}$$

$$\frac{\nu_x}{\nu_m} = \frac{2u_d}{u_x}. \tag{26}$$

The excitation of the "bending mode" requiring energy u_b starts as E^2 at low fields and saturates at $\eta\nu_m(u_b^-/u_b)^{1/2}$ at high fields. The excitation of the asymmetric stretching mode and nitrogen behaves as E^4 at low fields and saturates at $\xi\nu_m$. The electronic excitations start out as E^6 and increase as E^2 at high fields.

References

1. W. P. Allis and H. A. Haus, "Electron Distribution and Lasing Efficiency of Diatomic Gas Laser," Quarterly Progress Report No. 106, Research Laboratory of Electronics, M.I.T., July 15, 1972, pp. 49-60.

2. Ibid., see Eq. (22), p. 55.

B. INVERSION GROWTH RATE IN AN HF LASER AMPLIFIER

Joint Services Electronics Program (Contract DAAB07-71-C-0300)

J. R. Gersh

Measurements of the population inversion density for the v = 1 to v = 2 transition in an HF chemical laser amplifier at the time of peak gain have been made. Two different techniques are used, with fairly good agreement. From these measurements, we infer the rate at which the chemical reaction

$$F + H_2 \rightarrow HF + H \qquad (1)$$

creates the population inversion.

The experimental apparatus comprises an HF laser oscillator and amplifier employing identical discharge tubes, each with 60 pairs of 510 Ω resistors, whose leads act as pin electrodes. The pins are spaced 1 cm apart along the tube, with a 2.5 cm gap between opposite pins. The oscillator cavity is 1.5 m long, and is formed by a flat gold mirror and a dielectric-coated Germanium output mirror, with 5 m radius of curvature and 50% transmission. The two tubes are served by the same gas-handling system, which provides a flowing mixture of 193 Torr He, 6 Torr SF_6 and 1 Torr H_2.

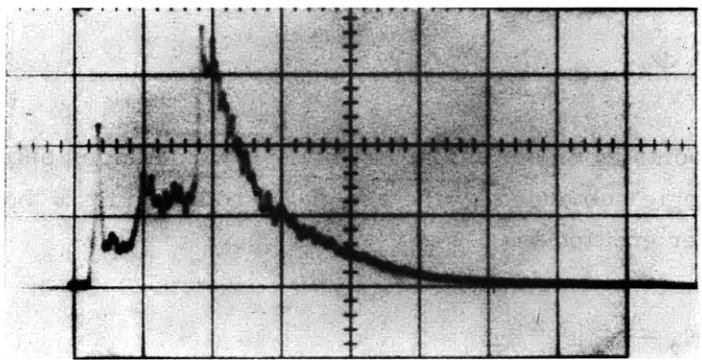

Fig. IV-2. Oscillator output pulse. Horizontal scale: 0.2 μs/div. Vertical scale: 0.2 V/div.

The timing of the oscillator output pulse may be varied, so that it may enter the amplifier at any time after the amplifier discharge. The optical signal is detected by a Ge:Au photoconductor cooled by LN_2, and is observed on a Tektronix 556 oscilloscope.

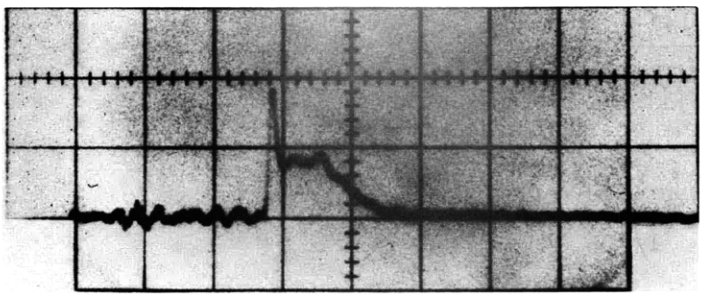

Fig. IV-3. Amplifier superradiant pulse. Oscilloscope sweep triggered by amplifier discharge current. Horizontal scale: 0.2 μs/div. Vertical scale: 10 mV/div.

Figure IV-2 shows a typical oscillator pulse with the amplifier turned off. The characteristic triple-peak shape represents three consecutive vibrational transitions: $v = 2 \rightarrow 1$, $v = 3 \rightarrow 2$, and $v = 1 \rightarrow 0$. The amplifier is superradiant. Figure IV-3 shows the amplifier superradiant pulse, which is also triple-peaked. Here the oscilloscope sweep is triggered by the amplifier discharge current. If the length of the amplifier is reduced to 30 pins, only the leading, $2 \rightarrow 1$ transition is superradiant. In this case the total superradiant power emitted is measured as 1.3 W, from which the inversion density may be calculated.

The active medium is modeled as a uniform rod of length ℓ and cross-sectional area A, with a particle density in the $v = 2$ level of N_2. The power emitted by spontaneous emission from a slice of length dz is then

$$dP = \frac{h\nu}{t_{sp}} N_2 A \, dz, \tag{2}$$

where t_{sp} is the spontaneous emission lifetime. If we consider only that fraction emitted through the solid angle subtended by the end of the rod, and let α be the small-signal gain, the total power emitted is

$$P = \int_0^{\ell} \frac{h\nu}{t_{sp}} N_2 \frac{A^2}{4\pi z^2} e^{\alpha z} \, dz. \tag{3}$$

For high-gain media such as HF this power will originate primarily in that section farthest from the output end:

$$P \approx \frac{h\nu}{t_{sp}} N_2 \frac{A^2}{4\pi \ell^2} \frac{1}{\alpha} e^{\alpha \ell}. \tag{4}$$

Since

$$\alpha = \frac{\lambda^2 (N_2 - N_1) \, g(\nu)}{8\pi t_{sp}}, \tag{5}$$

where $g(\nu)$ is the line-shape function, we get

$$P \approx \frac{2h\nu^3}{c^2} \left(\frac{N_2}{N_2 - N_1} \right) \frac{A^2}{\ell^2} \frac{1}{g(\nu)} e^{\alpha \ell} \tag{6}$$

or

$$N_2 - N_1 \approx \frac{8\pi t_{sp}}{\lambda^2 g(\nu)} \ln \left[P \frac{c^2 \ell^2 g(\nu)}{2h\nu^3 A^2} \left(\frac{N_2 - N_1}{N_1} \right) \right]. \tag{7}$$

The quantity $N_2 - N_1$ appears on both sides of Eq. 7, but on the right-hand side only in the slowly varying logarithmic factor, and only as a ratio of inversion to upper-state population. Hence a reasonable estimate of this ratio will yield a good value for the inversion itself. Chemiluminescence studies[1] indicate that the ratio of the reaction rate producing HF with v = 2 to that producing v = 1 is 3.26, thereby giving $N_2 - N_1/N_2 \approx 2/3$, with relaxation effects ignored. At line center $g(\nu)$ is equal to the inverse linewidth of the transition, which is taken[2] to be 1 GHz as an order-of-magnitude estimate. For the HF 2 → 1 transition observed here, $\lambda = 2.7\ \mu$ and $t_{sp} = 6.5$ ms.[3] The diameter of the active region around each pin has been measured as 0.25 in.,[4] which gives $A = 1.6\ cm^2$ and $\ell = 19$ cm. These values give $N_2 - N_1 = 1.3 \times 10^{15}\ cm^{-3}$. The superradiant pulse is observed at the time of peak gain in the amplifier, 560 ns after the start of the discharge current. In a chemical laser with an excess of one reactant, it may be assumed that the pumping rate into the i^{th} level goes as $R_i e^{-t/\tau}$, for an initial rate R_i, which indicates that the reaction slows down as the reactants are consumed. If we assume that the peak gain occurs when the reaction is essentially complete so that relaxation effects can take over, and take this time to be the 1/e point, we get $R_2 - R_1 = 3.7 \times 10^{21}\ cm^{-3}\ s^{-1}$.

Another method of calculating the inversion places reliance on direct measurements of the gain of the amplifier. Figure IV-4 shows the output of the amplifier

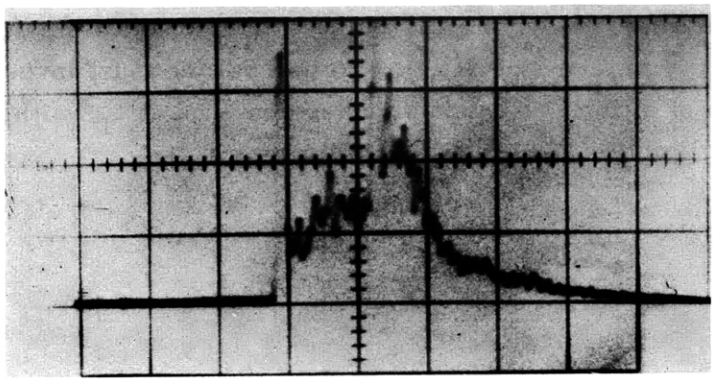

Fig. IV-4. Amplifier output. The input is a pulse similar to that in Fig. IV-2. Oscilloscope sweep triggered by amplifier discharge current. Horizontal scale: 0.2 μs/div. Vertical scale: 1 V/div.

at the time of peak gain, also with the sweep triggered by the amplifier discharge current. The amplitude may be compared with that shown in Fig. IV-2 to measure the gain. (The oscillator output is relatively stable in amplitude from pulse to pulse.) To determine the transient saturation effects, it is useful to note that the leading peak, whose gain we wish to relate to the inversion, is a very sharp spike, 40 ns wide. If

we assume that this time is short compared with that in which the pump can make a significant change in the populations, we can model the intensity of this radiation as an impulse. That is, we let I(t) be the limit as $\Delta t \to 0$ of a rectangular pulse of height $E/\Delta t$ and width Δt. E is then the area of this pulse, and represents the total energy, in J/cm^2, passing through the amplifier. In this model the rate equations for the v = 2 and v = 1 populations are

$$\frac{dN_2}{dt} = R_2(t) - (N_2 - N_1)\, W\, E\, \delta(t-t_1)$$

$$\frac{dN_1}{dt} = R_1(t) + (N_2 - N_1)\, W\, E\, \delta(t-t_1). \tag{8}$$

Combining them, letting $N = N_2 - N_1$ and $R = R_2 - R_1$, we obtain

$$\frac{dN}{dt} = R(t) - 2NWE\, \delta(t-t_1). \tag{9}$$

Here R_1 and R_2 are the rates at which the chemical reaction pumps these levels, t_1 is the time after the amplifier discharge of the $2 \to 1$ pulse, and $W = \frac{\lambda^2 g(\nu)}{8\pi h\nu t_{sp}}$. Relaxation is neglected; the primary method, HF-HF vibrational transfer,[4] has a lifetime at 1 Torr HF pressure of 11 μs that is long compared with any period of present interest.[5]

We let t_1^- be the time just before the pulse and t_1^+ be the time just after it, and we wish to find $N\left(t_1^+\right)$ in terms of $N\left(t_1^-\right)$. To do this, we must investigate Eq. 9 in detail. In the case of a finite rectangular pulse centered at t_1, with the pump considered to have negligible influence for small Δt, we have

$$\frac{dN}{dt} = -\frac{2NWE}{\Delta t} \qquad \text{for} \quad t_1 - \frac{\Delta t}{2} < t < t_1 + \frac{\Delta t}{2}, \tag{10}$$

and so

$$N\left(t_1^+\right) = N\left(t_1^-\right) e^{-2WE}. \tag{11}$$

To find the total energy extracted from the active medium by the laser pulse, we must integrate this change in population along the tube.

In a slice of thickness dz the energy extracted per unit area of the beam is

$$dE = \frac{h\nu \left\{N\left(t_1^-\right) - N\left(t_1^+\right)\right\}}{2}\, dz \tag{12}$$

and so

$$\frac{dE}{dz} = \frac{h\nu N\left(t_1^-\right)\left(1 - e^{-2WE}\right)}{2} . \tag{13}$$

Integrating (13) along the tube gives

$$N\left(t_1^-\right) = \frac{2}{\ell h\nu} \left\{ E_{out} - E_{in} + \frac{1}{2W} \ln \left(\frac{1 - \exp(-2WE_{out})}{1 - \exp(-2WE_{in})} \right) \right\} . \tag{14}$$

The beam diameter was measured as approximately 5 mm by closing an aperture until it was attenuated. The data of Figs. IV-2 and IV-4 yield $E_{in} = 1.4 \times 10^{-4}$ J/cm^2 and $E_{out} = 1.1 \times 10^{-3}$ J/cm^2, resulting in $N_2 - N_1 = 7.3 \times 10^{14}$ cm^{-3} and $R_2 - R_1 = 2.1 \times 10^{21}$ cm^{-3} s^{-1}.

The two methods agree within a factor of 2, which is not unreasonable, if we consider that some parameters were estimated. Based on the 3.26 pumping ratio mentioned above, and chemical studies[6] of the total reaction rate, $R_2 - R_1 = 7.2 \times 10^{21}$ cm^{-3} s^{-1}, under the assumptions of an initial concentration of 1 Torr H_2 and an order-of-magnitude estimate of 1 Torr F.

The inversion densities indicate that a total HF concentration of only $\approx 10^{15}$ cm^{-3} is produced. If all H_2 is consumed, we would expect $\approx$2 Torr, or $\approx 7 \times 10^{16}$ cm^{-3} to be produced. The following experiment, which was suggested by E. L. Frohring and conducted with him, indicates that only a fraction of the available H_2 is consumed.

The oscillator tube containing the same partial pressures of the gases as were present in the flowing mixture was sealed off. The oscillator was then pulsed repeatedly, using 36 pins at 2-s intervals. For 500 pulses the output intensity was observed to decrease approximately 0.1% per pulse. The volume of the tube is 1600 cm^3, that of the total active region around the pins is 29 cm^3. If all H_2 in this region were consumed at each pulse, the expected rate of intensity decrease would then be 1.8% per pulse. The lower rate indicates that only 1/9 Torr, or 4.0×10^{15} cm^{-3} is produced.

Further work will involve developing an applicable theory of transient saturation effects for a transition terminating in the ground state. The influence of the leading $2 \rightarrow 1$ peak of the oscillator pulse on the amplifier $v = 1$ population may then be related to the gain seen by the subsequent $1 \rightarrow 0$ peak. If this influence is traced through time, a direct measurement of the ratio of pumping rates into the $v = 2$ and $v = 1$ levels may be made.

References

1. J. C. Polanyi and D. C. Tardy, J. Chem. Phys. 51, 5717 (1969).

2. J. Goldhar, R. M. Osgood, and A. Javan, Appl. Phys. Letters 18, 167 (1971).
3. A. N. Chester and L. D. Hess, IEEE J. Quant. Electronics 8, 1 (1972).
4. S. Marcus and R. J. Carbone, IEEE J. Quant. Electronics 9, 651 (1972).
5. J. R. Airey and S. F. Fried, Chem. Phys. Letters 8, 23 (1971).
6. N. Cohen, "A Review of Rate Coefficients for Reactions in the H_2+F_2 Laser System," Technical Report TR-0172(2779)-2, Aerospace Corporation, El Segundo, California, September 1971. (AD737 553).

C. THE kDB SYSTEM AND THE OPTICS OF BIANISOTROPIC MEDIA

Joint Services Electronics Program (Contract DAAB07-71-C-0300)

J. A. Kong

It has long been recognized in the study of electrically anisotropic media such as uniaxial and biaxial crystals that a set of coordinates including propagation vector $\bar{k}$, electric vector $\bar{D}$, and magnetic vector $\bar{B}$ provides the most expedient scheme for dealing with them. When the medium is bianisotropic this system is indispensable. We have extended previous work[1-2] on anisotropic media to formulate the kDB system in a way that is useful for studying general anisotropic and bianisotropic media. In this report we first illustrate the use of the kDB system and then apply it to a biaxial crystal and a bianisotropic medium.

We write the constitutive relations for a bianisotropic medium first in DB representation.[3]

$$E_v = \kappa_{vw} D_w + \chi_{vw} B_w \tag{1a}$$

$$H_v = \gamma_{vw} D_w + \nu_{vw} B_w, \tag{1b}$$

where v, w denote x, y, z components and repeated indices imply summation. The three-dimensional constitutive matrices are then transformed to the kDB system.

$$\kappa_{ij} = t_{iv} t_{jw} \kappa_{vw}; \qquad \kappa_{vw} = t_{iv} t_{jw} \kappa_{ij} \tag{2a}$$

$$\chi_{ij} = t_{iv} t_{jw} \chi_{vw}; \qquad \chi_{vw} = t_{iv} t_{jw} \chi_{ij} \tag{2b}$$

$$\gamma_{ij} = t_{iv} t_{jw} \gamma_{vw}; \qquad \gamma_{vw} = t_{iv} t_{jw} \gamma_{ij} \tag{2c}$$

$$\nu_{ij} = t_{iv} t_{jw} \nu_{vw}; \qquad \nu_{vw} = t_{iv} t_{jw} \nu_{ij} \tag{2d}$$

where $i, j = 1, 2, 3$ denote components in the kDB system. The t_{iv} are elements of the transformation matrix.[4]

$$\overline{\overline{T}} = \begin{bmatrix} t_{1x} & t_{1y} & t_{1z} \\ t_{2x} & t_{2y} & t_{2z} \\ t_{3x} & t_{3y} & t_{3z} \end{bmatrix} \tag{3}$$

$$= \begin{bmatrix} \sin\phi & -\cos\phi & 0 \\ \cos\theta\cos\phi & \cos\theta\sin\phi & -\sin\theta \\ \sin\theta\cos\phi & \sin\theta\sin\phi & \cos\theta \end{bmatrix}. \tag{4}$$

The kDB system is defined by unit vectors $\hat{e}_1$, $\hat{e}_2$, and $\hat{e}_3$. The unit vector $\hat{e}_3$ points in the direction of $\bar{k}$. The unit vector $\hat{e}_2$ lies in the plane determined by $\hat{z}$ and $\bar{k}$, and is perpendicular to $\hat{e}_3$. The unit vector $\hat{e}_1$ is perpendicular to the plane determined by $\hat{z}$ and $\bar{k}$, and is therefore perpendicular to both $\hat{e}_3$ and $\hat{e}_2$. We can generate the kDB coordinate axes from the original coordinate axes by two successive rotations (Fig. IV-5).

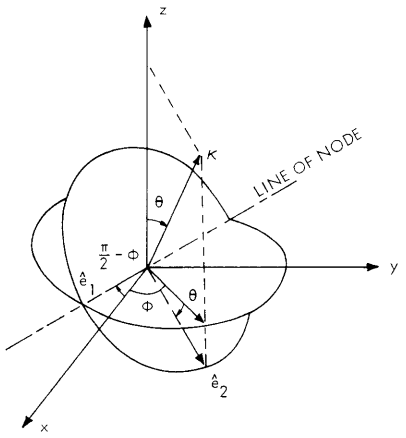

Fig. IV-5. Establishing the kDB system.

From Maxwell's equations, we obtain the equation for electric vector $\bar{D}$ in the kDB system.

$$\begin{bmatrix} D_1 \\ D_2 \end{bmatrix} = \frac{1}{[(u+\gamma_{12})(u-\gamma_{21})+\gamma_{11}\gamma_{22}][(u-\chi_{12})(u+\chi_{21})+\chi_{11}\chi_{22}]} \begin{bmatrix} u+\gamma_{12} & \gamma_{22} \\ -\gamma_{11} & u-\gamma_{21} \end{bmatrix}$$

$$\begin{bmatrix} \nu_{21} & \nu_{22} \\ -\nu_{11} & -\nu_{12} \end{bmatrix} \begin{bmatrix} u-\chi_{12} & -\chi_{22} \\ \chi_{11} & u+\chi_{21} \end{bmatrix} \begin{bmatrix} -\kappa_{21} & -\kappa_{22} \\ \kappa_{11} & \kappa_{12} \end{bmatrix} \begin{bmatrix} D_1 \\ D_2 \end{bmatrix}, \tag{5}$$

where $u = w/k$. Note also that in the kDB system $D_3 = 0$. Equation 5 is useful

for determining the normal modes in the medium and for obtaining the dispersion relations.

As a first example, consider a biaxial medium. Written in the principal coordinate system, we have

$$\bar{\bar{\kappa}} = \begin{bmatrix} \kappa_x & & \\ & \kappa_y & \\ & & \kappa_z \end{bmatrix} \tag{6a}$$

$$\bar{\bar{\nu}} = \nu \bar{\bar{I}} \tag{6b}$$

$$\bar{\bar{\chi}} = \bar{\bar{\gamma}} = 0. \tag{6c}$$

To relate to the permittivities, we note that $\kappa_x = 1/\epsilon_x$, $\kappa_y = 1/\epsilon_y$, and $\kappa_z = 1/\epsilon_z$. The impermeability ν is the reciprocal of μ. By using Eq. 3, the constitutive matrices can be transferred to the kDB system, and we obtain

$$\bar{\bar{\kappa}} = \begin{bmatrix} \kappa_x \sin^2\phi + \kappa_y \cos^2\phi & (\kappa_x-\kappa_y)\cos\theta\sin\phi\cos\phi & (\kappa_x-\kappa_y)\sin\theta\sin\phi\cos\phi \\ (\kappa_x-\kappa_y)\cos\theta\sin\phi\cos\phi & \left(\kappa_x\cos^2\phi+\kappa_y\sin^2\phi\right)\cos^2\theta+\kappa_z\sin^2\theta & \left(\kappa_x\cos^2\phi+\kappa_y\sin^2\phi-\kappa_z\right)\sin\theta\cos\theta \\ (\kappa_x-\kappa_y)\sin\theta\sin\phi\cos\phi & \left(\kappa_x\cos^2\phi+\kappa_y\sin^2\phi-\kappa_z\right)\sin\theta\cos\theta & \left(\kappa_x\cos^2\phi+\kappa_y\sin^2\phi\right)\sin^2\theta+\kappa_z\cos^2\theta \end{bmatrix}. \tag{7a}$$

$$\bar{\bar{\nu}} = \nu \bar{\bar{I}} \tag{7b}$$

$$\bar{\bar{\chi}} = \bar{\bar{\gamma}} = 0. \tag{7c}$$

Equation 5 yields

$$\begin{bmatrix} u^2-\nu\kappa_{11} & -\nu\kappa_{12} \\ -\nu\kappa_{12} & u^2-\nu\kappa_{22} \end{bmatrix} \begin{bmatrix} D_1 \\ D_2 \end{bmatrix} = 0. \tag{8}$$

Phase velocities of the characteristic waves can be immediately obtained by setting the determinant operating on $\bar{D}$ equal to zero.

$$u^2 = \frac{\nu}{2}\left[(\kappa_{11}+\kappa_{22}) \pm \left((\kappa_{11}-\kappa_{22})^2+4\kappa_{12}^2\right)^{1/2}\right]. \tag{9}$$

We obtain two $\bar{D}$ vectors corresponding to the two values for u^2. On the DB plane,

expressed in terms of the kDB base vectors $\hat{e}_1$ and $\hat{e}_2$, we have

$$\frac{D_2}{D_1} = \frac{\kappa_{12}}{u^2 - \nu\kappa_{22}} = \frac{2\kappa_{12}}{\kappa_{11} - \kappa_{22} \pm \left((\kappa_{11}-\kappa_{22})^2 + 4\kappa_{12}^2\right)^{1/2}}. \tag{10}$$

It can be shown that the two $\bar{D}$ vectors are orthogonal, since the scalar productor of the two vectors is zero.

Let

$$\tan 2\psi = 2\kappa_{12}/(\kappa_{11}-\kappa_{22}). \tag{11}$$

We observe from (11) that

$$\frac{D_2}{D_1} = \tan\psi \qquad \text{or} \quad -\cot\psi. \tag{12}$$

The two vectors are shown on the DB plane in Fig. IV-6. Equation 11 conforms with the known results through an Eulerian angle approach.[5] In the case of a uniaxial crystal

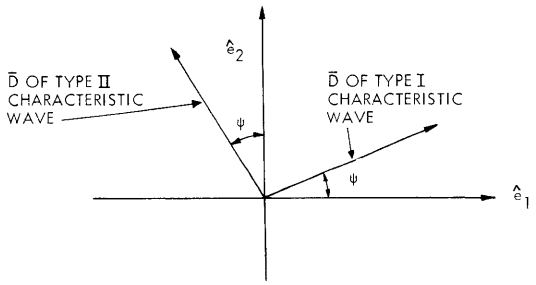

Fig. IV-6.
Characteristic waves in biaxial crystals.

with $\kappa_{12} = 0$, the $\bar{D}$ field vectors for the two characteristic waves coincide with the base vectors. None of the $\bar{E}$ vectors for the two waves lie on the DB plane. They both possess a component in the $\bar{k}$ direction. By definition, both waves are extraordinary waves (Type I and Type II). The Type I wave becomes an ordinary wave when the medium is uniaxial.

To give another example, we consider bianisotropic media that possess constitutive matrices

$$\overline{\overline{\kappa}} = \begin{bmatrix} \kappa & & \\ & \kappa & \\ & & \kappa_z \end{bmatrix} \tag{13a}$$

$$\overline{\overline{\nu}} = \begin{bmatrix} \nu & & \\ & \nu & \\ & & \nu_z \end{bmatrix} \tag{13b}$$

$$\overline{\overline{\chi}} = \overline{\overline{\gamma}}^{+} = \begin{bmatrix} 0 & \chi & 0 \\ -\chi & 0 & 0 \\ 0 & 0 & 0 \end{bmatrix}. \tag{13c}$$

In the kDB system, the constitutive matrices become

$$\overline{\overline{\kappa}} = \begin{bmatrix} \kappa & 0 & 0 \\ 0 & \kappa \cos^2\theta + \kappa_z \sin^2\theta & (\kappa-\kappa_z)\sin\theta\cos\theta \\ 0 & (\kappa-\kappa_z)\sin\theta\cos\theta & \kappa \sin^2\theta + \kappa_z \cos^2\theta \end{bmatrix} \tag{14a}$$

$$\overline{\overline{\nu}} = \begin{bmatrix} \nu & 0 & 0 \\ 0 & \nu \cos^2\theta + \nu_z \sin^2\theta & (\nu-\nu_z)\sin\theta\cos\theta \\ 0 & (\nu-\nu_z)\sin\theta\cos\theta & \nu \sin^2\theta + \nu_z \cos^2\theta \end{bmatrix} \tag{14b}$$

$$\overline{\overline{\chi}} = \overline{\overline{\gamma}}^{+} = \begin{bmatrix} 0 & \chi\cos\theta & \chi\sin\theta \\ -\chi\cos\theta & 0 & 0 \\ -\chi\sin\theta & 0 & 0 \end{bmatrix}. \tag{14c}$$

Equation 5 yields

$$(u-\chi\cos\theta)^2 \begin{bmatrix} D_1 \\ D_2 \end{bmatrix} = \begin{bmatrix} \kappa\left(\nu\cos^2\theta + \nu_z\sin^2\theta\right) & 0 \\ 0 & \nu\left(\kappa\cos^2\theta + \kappa_z\sin^2\theta\right) \end{bmatrix} \begin{bmatrix} D_1 \\ D_2 \end{bmatrix}. \tag{15}$$

Table IV-1. Electromagnetic fields for a bianisotropic medium.

Characteristic Waves / Field Vectors	Type I Wave	Type II Wave
$\bar{D}$	$\begin{bmatrix} 1 \\ 0 \\ 0 \end{bmatrix}$	$\begin{bmatrix} 0 \\ 1 \\ 0 \end{bmatrix}$
$\bar{B}$	$\begin{bmatrix} 0 \\ \kappa/(u-\chi\cos\theta) \\ 0 \end{bmatrix}$	$\begin{bmatrix} -(u-\chi\cos\theta)/\nu \\ 0 \\ 0 \end{bmatrix}$
$\bar{E}$	$\begin{bmatrix} \kappa u/(\nu-\chi\cos\theta) \\ 0 \\ 0 \end{bmatrix}$	$\begin{bmatrix} 0 \\ (u-\chi\cos\theta)/\nu \\ \frac{\chi}{\nu}(u-\chi\sin\theta)+(\kappa_z-\kappa)\cos\theta\sin\theta \end{bmatrix}$
$\bar{H}$	$\begin{bmatrix} 0 \\ u \\ \left(-\chi+\frac{\kappa(\nu_z-\nu)\cos\theta}{u-\chi\cos\theta}\right)\sin\theta \end{bmatrix}$	$\begin{bmatrix} -u \\ 0 \\ 0 \end{bmatrix}$
u	$\chi\cos\theta \pm \sqrt{\kappa\left(\nu\cos^2\theta+\nu_z\sin^2\theta\right)}$	$\chi\cos\theta \pm \sqrt{\nu\left(\kappa\cos^2\theta+\kappa_z\sin^2\theta\right)}$
Dispersion Relation (in EB base)	$k_t^2+\frac{m^2}{pq_z}k_z^2=\frac{1}{pq_z}\left(p\frac{\omega}{c}-\ell k_z\right)^2$	$k_t^2+\frac{p_z}{p}k_z^2=\frac{p_z}{m^2p}\left(p\frac{\omega}{c}-\ell k_z\right)^2$

The phase velocities of the two characteristic waves can be easily obtained from (15). Other field components and the dispersion relations are summarized in Table IV-1.

References

1. A. Sommerfeld, Optics (Academic Press, Inc., New York, 1964).
2. L. D. Landau and E. M. Lifshitz, Electrodynamics of Continuous Media (Pergamon Press, New York, 1960).
3. J. A. Kong, "Theorems of Bianisotripic Media," Proc. IEEE 60, 1036-1046 (1972).
4. L. D. Landau and E. M. Lifshitz, Mechanics (Addison-Wesley Publishing Company, South Reading, Mass., 1960), p. 110.
5. J. A. Kong, "Biaxial Crystal Optics," J. Opt. Soc. Am. 61, 49-52 (1971).

D. EMISSIVITY AND REFLECTION COEFFICIENTS FOR STRATIFIED EARTH MEDIA

Joint Services Electronics Program (Contract DAAB07-71-C-0300)

J. A. Kong, P. S. K. Wong, D. Pao

In remote sensing of thermal radiation at GHz range, the apparent temperature of an object originates from the sum of two components: a component that is due to reflection of illumination from a variety of sources, and a component that is due to thermal emission from the object. We associate with the first component a temperature T_r. Assume that the temperature T_i represents the incident intensity of the external sources such as that attributable to the atmosphere and that to the 3.5°K cosmic radiation background. If the reflectivity, r, of the object is determined, then $T_r = rT_i$. If the thermal temperature of the observed body is T_h, then the other component because of thermal emission is equal to eT_h, where e is the emissivity. By reciprocity, $e = 1 - r$. Physically, a perfect absorber with $r = 0$ such as a blackbody is also a perfect emitter, while a perfect reflector with $r = 1$ does not emit. Thus we can write the brightness temperature of the body as

$$T_b = eT_h + (1-e)T_i. \tag{1}$$

We shall calculate reflection coefficients, and therefore reflectivities of a plane stratified medium composed of n layers with different physical properties and depths. From the reflection coefficients, the emissivities and apparent temperatures can also be determined. We consider the n-layer plane stratified medium as shown in Fig. IV-7.

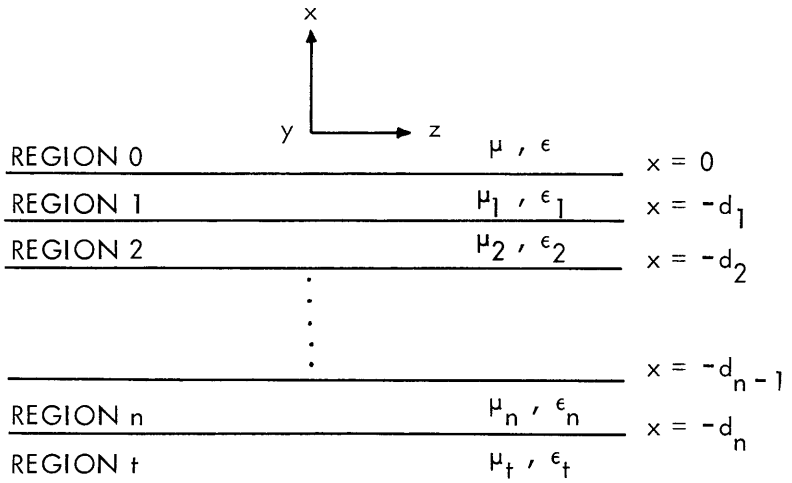

Fig. IV-7. Stratified medium.

Let the x-z plane be the plane of incidence. The boundaries are situated at $x = 0, -d_1, \ldots -d_n$. The $(n+1)^{th}$ region is semi-infinite and is labeled Region t. All of the permittivities ϵ_i and the permeabilities μ_i can be real as well as imaginary. We wish to determine the reflection coefficients for this structure and express field solutions in all regions in terms of the reflection coefficients. The reflectivities, as well as the emissivities, can be calculated from the reflection coefficients.

Let all regions be isotropic. Then a wave of arbitrary polarization can be decomposed into two polarization components. The component with the $\overline{E}$ vector perpendicular to the plane of incidence is referred to as perpendicular or horizontal polarization, or as a TE wave or an s-wave. The component with the $\overline{E}$ vector parallel to the plane of incidence is referred to as parallel or vertical polarization, or as a TM wave or a p-wave. The p-wave component has its $\overline{H}$ field perpendicular to the plane of incidence. To distinguish the two components, we use subscript p to denote the p-wave and subscript s for the s-wave.

The total reflection coefficient attributable to the stratified medium as a whole is determined to be

$$R = \left\{ \frac{1}{R_{01}} + \Big/ \frac{R_{01}^2 - 1}{R_{01}} + R_{01}^2 \exp(i2k_{1x}d_1) \left\{ \frac{1}{R_{12}} + \Big/ \frac{R_{12}^2 - 1}{R_{12}} \right.\right.$$

$$+ R_{12}^2 \exp[i2k_{2x}(d_2 - d_1)] \left\{ \frac{1}{R_{23}} + \Big/ \frac{R_{23}^2 - 1}{R_{23}} + \ldots \right.$$

$$\left.\left.\left. + R_{(n-1)n}^2 \exp[i2k_{nx}(d_n - d_{n-1})]\, R_{nt} \right\} \ldots \right\} \right\}. \qquad (2)$$

Equation 2 is a closed-form solution for the reflection coefficient R in continuous fractions. The s- and p-wave components can be distinguished by associating subscripts s and p to the individual Fresnel reflection coefficient $R_{\ell(\ell+1)}$.

The emissivity, e, of the stratified medium is

$$e = 1 - |R|^2, \qquad (3)$$

where $r = |R|^2$ is the reflectivity, and R is given by Eq. 2.

In Fig. IV-8, we show the emissivity of snow-covered land viewed from the nadir. The model has 7 layers. There are 6 layers of snow with increasing density from $\rho_1 = 0.1$ to $\rho_6 = 0.6$ with increments of 0.1 on top of land with permittivity $\epsilon_t = 5\epsilon_0$. The permittivities of the snow are determined from

$$\epsilon_i = (3.2)^{1.09\rho_i} + i(0.001)\rho_i. \qquad (4)$$

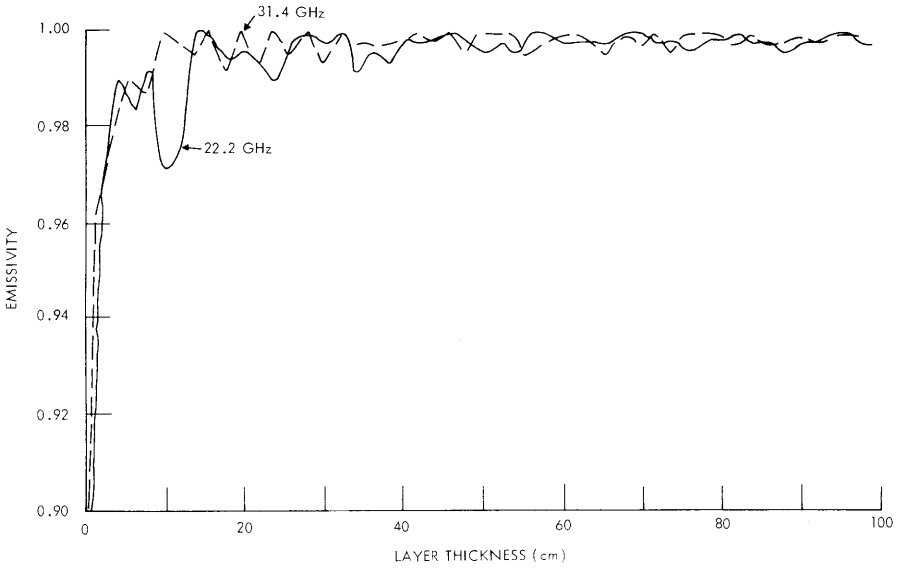

Fig. IV-8. Emissivity of snow-covered land.

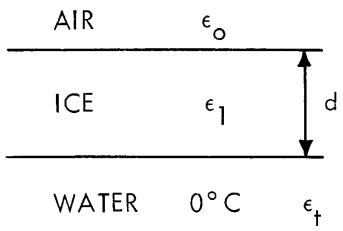

Fig. IV-9. Model of ice-covered water.

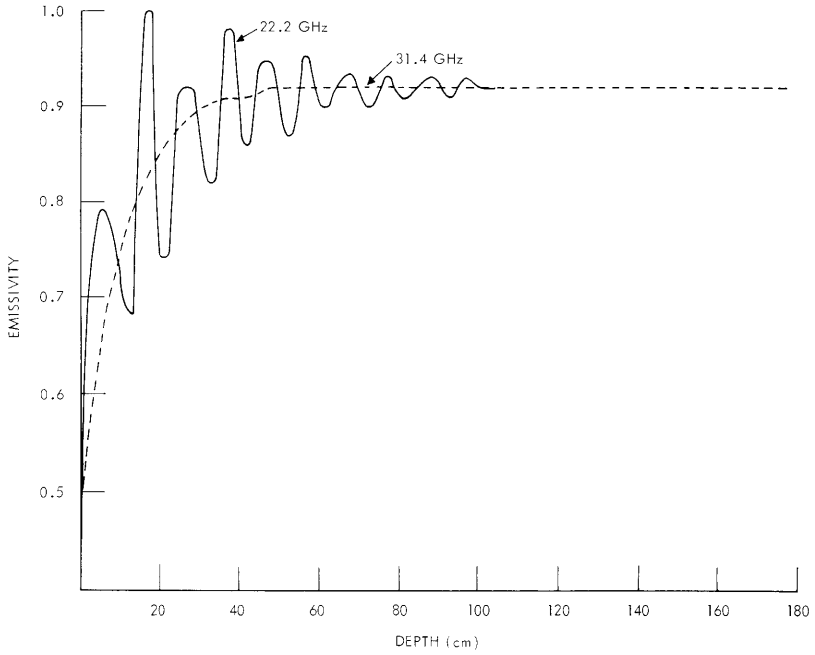

Fig. IV-10. Emissivity of ice-covered sea water.

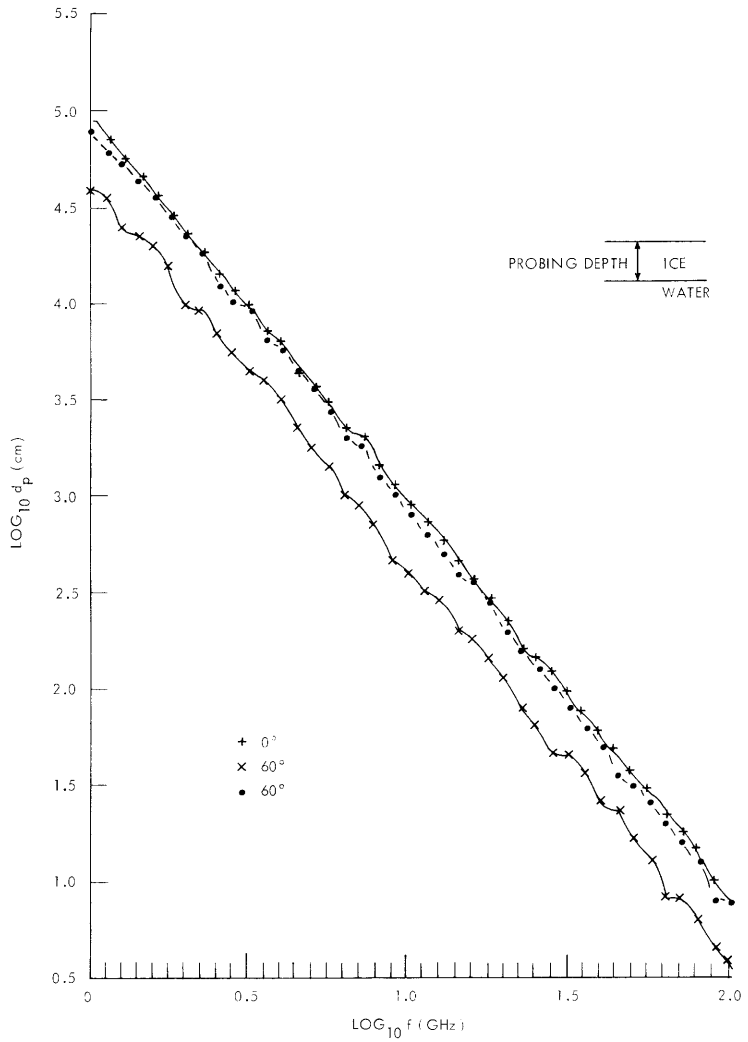

Fig. IV-11. Probing depth for ice over water as a function of frequency.

which is a simple formula[1] for air-snow mixture. All layers have the same thickness, d. The diagram is plotted for emissivity as a function of d, the common layer thickness. The computer program can be used for arbitrary combination of layer permittivities and layer thicknesses.

We shall now consider a simple two-layer model of ice-covered water (Fig. IV-9). The permittivity for ice is taken as[2]

$$\epsilon_1 = 3.2 + iAf,$$

where $A = 6.4 \times 10^{-4}$ GHz, and f is the frequency in GHz. The imaginary part of ϵ_1

represents resonance absorption which is true for f > 1 GHz. Note that the Debye absorption is negligible compared with this resonance absorption. To calculate the permittivity for sea water, we use a Debye equation.[3]

In Fig. IV-10 we show the emissivity for ice-covered sea (assuming a salinity of 4% and temperature 0°C) plotted as a function of ice depth viewed from the nadir. The permittivity for ice is $\epsilon_1 = 3.2 + i0.014$; for sea water at 22.2 GHz, $\epsilon_t = 16.4 + i28.7$, and at 31.4 GHz, $\epsilon_1 = 3.2 + i0.02$, $\epsilon_t = 11.1 + i21.8$. The dashed line is plotted for 31.4 GHz frequency, and the solid line for 22.2 GHz frequency. It can be seen that the emissivity damps to a constant value, where the presence of the bottom layer (sea water) cannot be sensed.

It is interesting to investigate to what depth the subsurface can be probed with microwaves from remote sensing. We define the probing depth d_p as the depth of the layer when $e(d_p)/e(\infty)$ reaches a constant value, 1. Figure IV-11 shows a plot of depth d_p (in cm) against frequency f (in GHz). Both scales are logarithmic. The viewing angles are at $\theta = 0°$ (the nadir) and at $\theta = 60°$. It can be seen that the probing depth with TE fields is greater than with TM waves at each frequency, and that the slopes of the curves are almost constant.

References

1. T. Yoshino, "The Reflection Properties of Radio Waves on the ICE Cap," IEEE Trans., Vol. AP-15, No. 4, pp. 542-551, 1967.
2. M. E. R. Walford, "Field Measurements of Dielectric Absorption in Antarctic Ice and Snow at Very High Frequencies," J. Glaciol. 7, 89 (1968).
3. J. A. Saxton, "Electrical Properties of Sea Water," Wireless Engr. 29, 269-275 (1952).

E. GEOPHYSICAL PROBING WITH DIPOLE ANTENNAS

Joint Services Electronics Program (Contract DAAB07-71-C-0300)

J. A. Kong, L. Tsang

When using electromagnetic waves in geophysical probing, antennas that are used as sources can usually be treated as dipoles. The terrestrial areas under examination are modeled, most of the time, as a plane stratified medium. The problem of electromagnetic field radiation of dipole antennas in the presence of stratified anisotropic media has been solved for various dipole sources and for stratified anisotropic earth.[1] The solutions are obtained without using the conventional Hertzian potential functions. The results are expressed in the form of integral representations.

Assume that the antenna source is at an elevation d_o from the surface of the

stratified medium. Choose a cylindrical coordinate system such that the dipole source is at the origin and the z axis is perpendicular to the planes of stratification. Use ρ to denote distance transverse to the z direction and ϕ for azimuthal angles. When the antennas are horizontal, we take ϕ to be zero along the direction of the antenna. When the antennas are vertical, we have circular symmetry and the solution is independent of ϕ. The solutions for the field components can, in turn, be expressed in terms of certain basic integrals. In $z > d_o$ regions, the results are as follows.

Vertical Electric Dipole

$$J_{ve} = \int_{-\infty}^{\infty} dk_\rho \frac{k_\rho}{k_z^{(e)}} (1+R^{TM}) H_o^{(1)}(k_\rho \rho) \exp\left(ik_z^{(e)} z\right). \tag{1}$$

Vertical Magnetic Dipole

$$J_{vm} = \int_{-\infty}^{\infty} dk_\rho \frac{k_\rho}{k_z^{(m)}} (1+R^{TE}) H_o^{(1)}(k_\rho \rho) \exp\left(ik_z^{(m)} z\right). \tag{2}$$

In these expressions, superscripts TE and TM denote transverse electric and transverse magnetic components, respectively. The subscripts on J (ve, vm) signify the kinds of dipoles with which we are dealing. R^{TE} and R^{TM}, the reflection coefficients for the TE and TM components, are expressed in terms of continuous fractions.[1] The ρ component of the wave vector $\bar{k}$ is k_ρ and its z component is k_z. Superscripts (e) and (m) on k_z represent the effects of electric and magnetic anisotropy of the stratified medium.

We can define four vector operators in terms of these basic integrals to obtain all electromagnetic field components. We write the operators in the form of column matrices.

$$\nabla_{v1} = \begin{bmatrix} 0 \\ \partial/\partial\rho \\ 0 \end{bmatrix} \tag{3}$$

$$\nabla_{v2} = \begin{bmatrix} \partial^2/\partial z \partial \rho \\ 0 \\ k^2 + \partial^2/\partial z^2 \end{bmatrix}. \tag{4}$$

Then the results are as follows.

Vertical Electric Dipole

$$\bar{E}^{TM} = \left(-\frac{I\ell}{8\pi\omega\epsilon}\right)\nabla_{v2}J_{ve} \tag{5a}$$

$$\bar{H}^{TM} = \left(-i\,\frac{I\ell}{8\pi}\right)\nabla_{v1}J_{ve} \tag{5b}$$

$$\bar{E}^{TE} = \bar{H}^{TE} = 0. \tag{5c}$$

Vertical Magnetic Dipole

$$\bar{E}^{TE} = \left(\frac{IA\omega\mu}{8\pi}\right)\nabla_{v2}J_{vm} \tag{6a}$$

$$\bar{H}^{TE} = \left(-i\,\frac{IA}{8\pi}\right)\nabla_{v1}J_{vm} \tag{6b}$$

$$\bar{E}^{TM} = \bar{H}^{TM} = 0. \tag{6c}$$

In these expressions $I\ell$ denotes the strength of the electric dipoles, and IA the strength of the magnetic dipoles. We see that once the basic integrals of a given dipole in the

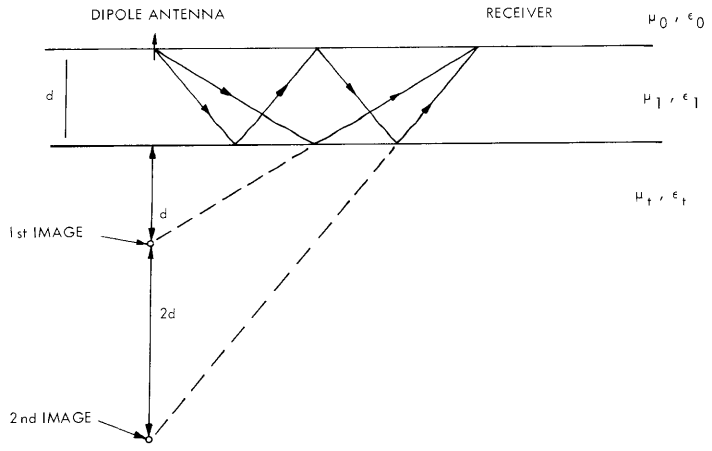

Fig. IV-12. Probing the subsurface with a dipole antenna.

presence of a given stratified profile are solved analytically, the field solutions can readily be obtained by differentiation of the basic integrals. We shall consider vertical dipoles laid on the surface of a two-layer medium (Fig. IV-12).

In geophysical probing with the interference fringe method, the dipoles and

the observation points are on the surface. We can expand $1 + R^{TM}$ and $1 + R^{TE}$ in power series.

$$1 - R^{TM} = \left(1+R_{01}^{TM}\right)\left[1 + \left(1+R_{10}^{TM}\right) \sum_{m=1}^{\infty} \left(R_{10}^{TM}\right)^{m-1} \left(R_{12}^{TM}\right)^{m} \exp(i2k_{iz}md)\right] \tag{7a}$$

$$1 + R^{TE} = \left(1+R_{01}^{TE}\right)\left[1 + \left(1+R_{10}^{TE}\right) \sum_{m=1}^{\infty} \left(R_{10}^{TE}\right)^{m-1} \left(R_{12}^{TE}\right)^{m} \exp(i2k_{iz}md)\right]. \tag{7b}$$

Each term in the summation can be evaluated by the saddle-point method and attributed to a particular image source (Fig. IV-12). The transmitting antenna radiates in all directions. The wave that reaches the receiver without reflection from the subsurface corresponds to the first term in both expressions. Thus, the first term is the classic half-space solution.

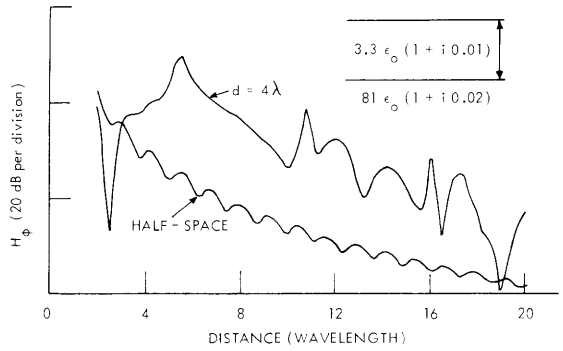

Fig. IV-13. Interference patterns for H_ϕ component of a vertical electric dipole.

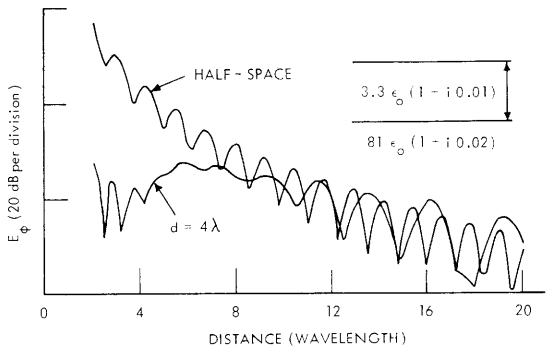

Fig. IV-14. Interference patterns for E_ϕ component of a vertical magnetic dipole.

The wave that arrives at the receiver after one reflection from the subsurface can be traced back to the first image in Fig. IV-12 and is identified with the first term in the summation series in Eq. 7. Similarly, the plane wave that arrives at the receiver after n reflections from the subsurface is represented by the n^{th} image and corresponds to the n^{th} term in the summation series.

In Figs. IV-13 and IV-14 we illustrate the interference patterns for H_ϕ of a vertical electric dipole and E_ϕ of a vertical magnetic dipole. If there is no subsurface

reflector the spatial wavelength of the interference pattern λ_{int} is related to the refraction index n_t of the half-space medium by $n_t = 1 + \lambda_o/\lambda_{int}$, where λ_o is the free-space wavelength corresponding to the transmitting antenna frequency. From measurements of λ_{int} we can estimate the value of the index of refraction of the half-space medium. The overall patterns from a water subsurface are also illustrated in Figs. IV-13 and IV-14. The first peak in the interference patterns for two-layer media occurs at approximately 6λ which can be attributed to waves reflected from the subsurface at the critical angle in the first medium.

References

1. J. A. Kong, Geophys. 37, 985-996 (1972).

F. A SIMPLIFIED CIRCUIT MODEL FOR MICROSTRIP

National Science Foundation (Grant GK-31012X), Cornell University
Joint Services Electronics Program (Contract DAAB07-71-C-0300)

H. J. Carlin

The advantage of a network model for a physical structure is that the model, if correctly established, implicitly contains the physical constraints of the actual system, and these constraints need not subsequently be called into play for every new case. A recent example is the case of coupled lines[1] to model longitudinally uniform but transversely inhomogeneous waveguides. The network model for a cylindrical waveguide loaded concentrically with a dielectric rod comprised a TE and a TM transmission line coupled together and the properties of this model established that, surprisingly, the lossless waveguide structure could support complex eigenvalues as well as backward waves. The general network idea stems from Schelkunoff[2] who established that uniform guide structures can be represented by an infinite number of coupled TE and TM transmission lines. The practical approximating network model is obtained by appropriately truncating the infinite Schelkunoff representation.[1]

In this report we show how a pair of coupled lines can give an extremely simple and useful model for Microstrip dispersion. We take a TEM transmission line and a TE line and form a distributed circuit with these 2 lines coupled together. The uncoupled lines propagate the ordinary TEM and TE modes. The coupled circuit automatically represents a pair of modes which are no longer TEM or TE but instead are the two lowest order hybrid modes that exist on the strip line. In effect, circuit theory does the work in producing the required modes.

The pair of coupled lines modeling the Microstrip is shown in Fig. IV-15. The

circuit model for the physical structure is based on the fact that TEM and TE type modes excite each other by virtue of the presence of the dielectric substrate. It is

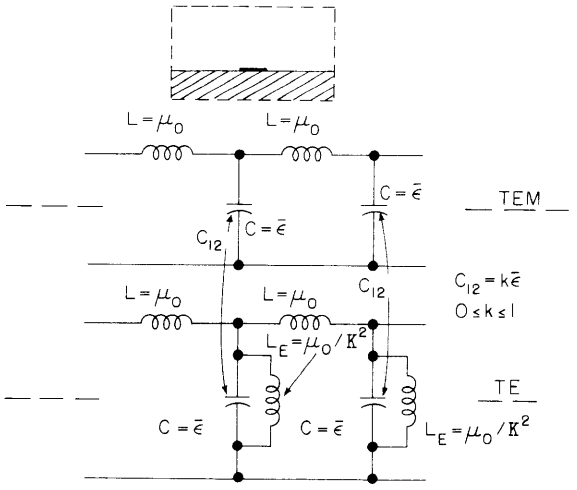

Fig. IV-15.
TEM-TE Network model for Microstrip (per unit length).

also assumed in the model that the uncoupled TEM and TE modes propagate at the same velocity at very high frequencies, i.e., there is a common value of $\bar{\epsilon}$ for both coupled lines.

The series impedance and shunt admittance matrices per unit length for the pair of coupled lines in Fig. IV-15 are

$$Z = p\mu_o \begin{bmatrix} 1 & 0 \\ 0 & 1 \end{bmatrix}, \quad Y = p\epsilon_o \begin{bmatrix} \bar{\epsilon} & c_{12} \\ c_{12} & \bar{\epsilon} \end{bmatrix} + \frac{1}{\mu_o p} \begin{bmatrix} 0 & 0 \\ 0 & \mathcal{K}^2 \end{bmatrix}. \tag{1}$$

Here $p = \sigma + j\omega$ is complex frequency, and ϵ_o, μ_o are the constitutive constants of free space. There are only three constants that determine the circuit model: $\bar{\epsilon}$, the effective static dielectric constant for the network model, $\mathcal{K}$, the cutoff wave number for the uncoupled TE mode, and the coupling capacitance $c_{12} = k\bar{\epsilon}$, where $0 \leq k \leq 1$ is the capacitive coefficient of coupling. The effective dc dielectric constant is given by the static relation

$$\bar{\epsilon} = \left(\frac{z_o}{\bar{z}_o} \right)^2, \tag{2}$$

where the characteristic impedances of the Microstrip are z_o with air dielectric, $\bar{z}_o$ with substrate relative dielectric constant ϵ_s. The program MSTRIP[3] is used for the static calculation of z_o, $\bar{z}_o$. The squared eigenvalues γ^2 associated with ZY are given

in normalized form as

$$-\frac{\gamma^2}{\mathscr{K}^2} = \Omega^2 - \frac{1}{2} \pm \sqrt{k^2\Omega^4 + \frac{1}{4}}. \tag{3}$$

The normalized angular frequency is

$$\Omega = \frac{\omega}{\omega_c}, \qquad \omega_c = \frac{\mathscr{K} v_o}{\sqrt{\bar{\epsilon}}}, \tag{4}$$

where ω_c is the cutoff frequency of the uncoupled TE line, and the free-space velocity is

$$v_o = \frac{1}{\sqrt{\mu_o \epsilon_o}}.$$

The relative effective dielectric constant is

$$\epsilon_e(\omega) = \left(\frac{v_o}{v(\omega)}\right)^2, \qquad v^2(\omega) = -\frac{\omega^2}{\gamma^2}, \tag{5}$$

where $v(\omega)$ is the phase velocity of propagation in the Microstrip corresponding to the plus sign in the dispersion relation (3). This mode propagates down to dc. The other mode (minus sign in (3)) is cut off at low frequencies. Then from (3), (4), and (5)

$$\epsilon_e = -\left(\frac{\gamma^2}{\omega^2}\right) \cdot v_o^2 = \bar{\epsilon} - \frac{\mathscr{K}^2 v_o^2}{2\omega^2} + \sqrt{(k\bar{\epsilon})^2 + \left(\frac{\mathscr{K}^2 v_o^2}{2\omega^2}\right)^2}. \tag{6}$$

Thus we verify that $\epsilon_e(0) = \bar{\epsilon}$.

The second constant, the coefficient of coupling k, is easily found if we assume that at high frequencies all energy of the propagating mode is in the substrate, i.e., $\epsilon_e(\infty) = \epsilon_s$, the substrate dielectric constant. Thus from (6)

$$k = \frac{\epsilon_s - \bar{\epsilon}}{\bar{\epsilon}}. \tag{7}$$

There is only one more parameter to be determined, the TE cutoff wave number $\mathscr{K}$. This is found by equating the frequency for the point of inflection ω_i calculated from (6), with the value given by Getsinger.[4] From (6) we set

$$\frac{d^2\epsilon_e}{d\omega^2} = 0,$$

which yields

$$\frac{\omega_i^2}{\omega_c^2} = \frac{R}{k}, \qquad R = \frac{(2\sqrt{7}-1)^{1/2}}{6}. \tag{8}$$

The Getsinger[4] equation gives

$$\omega_i = \frac{\bar{z}_o}{2\mu_o b\sqrt{3G}},$$

where b is the substrate thickness, and G is a semiempirical parameter that depends

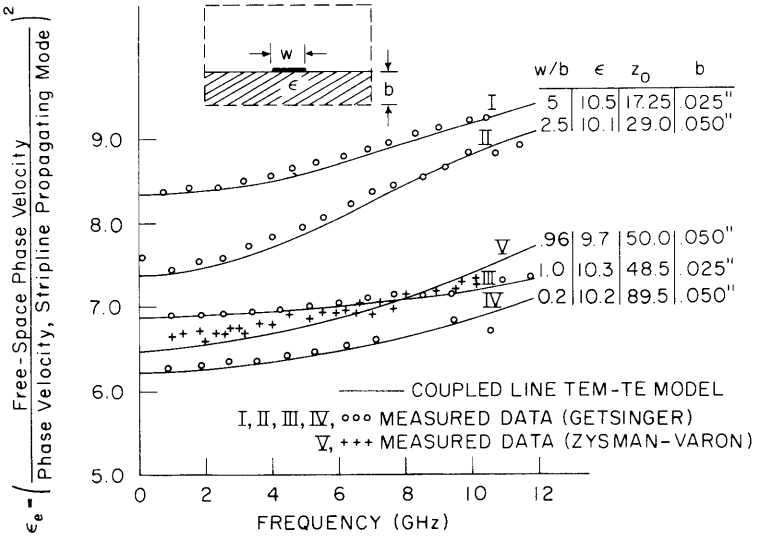

Fig. IV-16. Theoretical vs experimental dispersion curves for Microstrip.

on $\bar{z}_o$. In our circuit model for best fit we use the relation for G (differing from Getsinger[4])

$$G = .500 + .001\,\bar{z}_o^{3/2}. \tag{9}$$

Then from (8)

$$\mathcal{K}^2 = \frac{k}{R}\,\frac{(2\pi)^2}{12Gb^2}\,\bar{\epsilon}\left(\frac{\bar{z}_o}{376.7}\right)^2. \tag{10}$$

Our circuit model is now completely determined from the Microstrip geometry and the dielectric constant ϵ_s of the substrate. No interpolation to specific experimental dispersion data is required as in Getsinger's model.[4]

Figure IV-16 shows dispersion curves calculated from our simple 2-coupled line model and compared with experimental data.[4, 5] The simple network model fits the Getsinger data very well. The same model also fits the measured dispersion data of Zysman and Varon.[5]

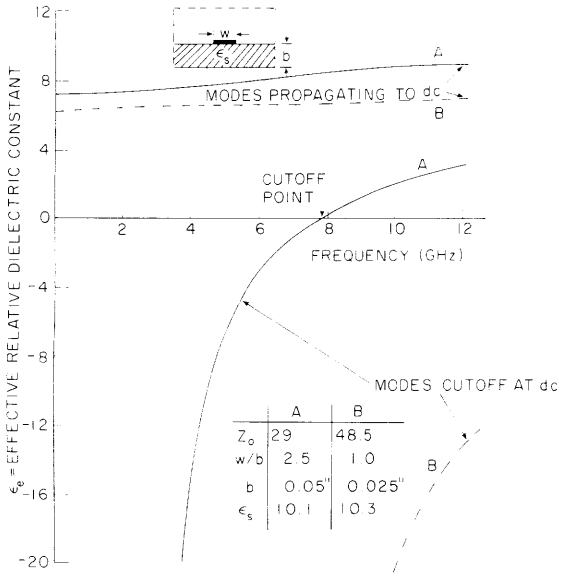

Fig. IV-17.
Modes in Microstrip (TEM-TE model).

Figure IV-17 compares dispersion curves calculated from the model for the mode that propagates to dc and the mode that is cut off below a finite frequency. Note that, as we would expect, the mode that is cut off at dc exhibits a higher and higher cutoff frequency as its paired propagating mode becomes less dispersive in character.

Helpful discussions with Professors Paul Penfield of M. I. T., and Paul McIsaac of Cornell University are acknowledged with thanks.

References

1. D. F. Noble and H. J. Carlin, "Circuit Properties of Coupled Dispersive Transmission Lines," IEEE Trans., Vol. CT-20, No. 1, pp. 56-64, January 1973.

2. S. A. Schelkunoff, "Generalized Telegraphist's Equations for Wave Guides," Bell System Tech. J. 31, 784-801 (1952).

3. T. G. Bryant and J. A. Weiss, "MSTRIP," IEEE Trans., Vol. MTT-19, pp. 418-419, April 1971.

4. W. Getsinger, "Microstrip Dispersion Model," IEEE Trans., Vol. MTT-21, No. 1, pp. 34-39, January 1973.

5. G. Zysman and B. Varon, "Wave Propagation in Microstrip Transmission Lines," 1969 G-MTT Symposium Digest, pp. 3-9.